Virology 432 (2012) 485–494

Contents lists available at SciVerse ScienceDirect

Virology

journal homepage: www.elsevier.com/locate/yviro

Coronavirus E protein forms ion channels with functionally and structurally-involved membrane lipids

Carmina Verdiá-Báguena [a,1], Jose L. Nieto-Torres [b,1], Antonio Alcaraz [a], Marta L. DeDiego [b], Jaume Torres [c], Vicente M. Aguilella [a,*], Luis Enjuanes [b,*]

[a] Department of Physics, Laboratory of Molecular Biophysics, Universitat Jaume I, 12071 Castellón, Spain
[b] Department of Molecular and Cell Biology, Centro Nacional de Biotecnología (CNB-CSIC), Campus Universidad Autónoma de Madrid, Darwin 3, 28049 Madrid, Spain
[c] School of Biological Sciences, Division of Structural and Computational Biology, Nanyang Technological University, Singapore 637551, Singapore

ARTICLE INFO

Article history:
Received 11 May 2012
Returned to author for revisions
6 June 2012
Accepted 6 July 2012
Available online 24 July 2012

Keywords:
Coronavirus
SARS
Envelope protein
Ion channel
HCoV-229E
Lipid membranes

ABSTRACT

Coronavirus (CoV) envelope (E) protein ion channel activity was determined in channels formed in planar lipid bilayers by peptides representing either the transmembrane domain of severe acute respiratory syndrome CoV (SARS-CoV) E protein, or the full-length E protein. Both of them formed a voltage independent ion conductive pore with symmetric ion transport properties. Mutations N15A and V25F located in the transmembrane domain prevented the ion conductivity. E protein derived channels showed no cation preference in non-charged lipid membranes, whereas they behaved as pores with mild cation selectivity in negatively-charged lipid membranes. The ion conductance was also controlled by the lipid composition of the membrane. Lipid charge also regulated the selectivity of a HCoV-229E E protein derived peptide. These results suggested that the lipids are functionally involved in E protein ion channel activity, forming a protein–lipid pore, a novel concept for CoV E protein ion channel entity.

Introduction

Coronaviruses (CoV) are vertebrate pathogens that cause common colds, bronchiolitis and acute respiratory distress syndrome that may lead to death in humans, and lethal diseases of high economic importance in animals (Perlman and Netland, 2009). In fact, their relevance increased when the causative agent of the severe acute respiratory syndrome (SARS) was identified as a CoV. SARS-CoV emerged at the end of 2002 in Guangdong province, China, causing an epidemic with 8000 infected people and a death rate close to 10% (Drosten et al., 2003; Rota et al., 2003). SARS-CoV like viruses have been identified in bat reservoirs all over the world (Chu et al., 2008; Drexler et al., 2010; Muller et al., 2007; Quan et al., 2010), making SARS-CoV reemergence a realistic possibility.

Members of the *Coronaviridae* family (de Groot et al., 2012) have a plus-strand RNA genome of around 30 kb in length (Enjuanes et al., 2008). CoV viral genome is packed by the nucleocapsid (N) protein, to form a helicoidal nucleocapsid that is protected by a lipid envelope. Several viral proteins, including the spike (S), envelope (E), and membrane (M) proteins are embedded within this lipid envelope. In addition, a variable set of proteins is also present within the membrane, depending on the CoV species. In the case of SARS-CoV, proteins 3a, 6, 7a and 7b have also been identified in the viral membrane (Huang et al., 2006, 2007; Schaecher et al., 2007; Shen et al., 2005).

CoV E protein is a small transmembrane protein of between 76 and 109 amino acids in length (Arbely et al., 2004; Raamsman et al., 2000). E protein amino acid sequence is quite divergent among different CoVs, nevertheless its predicted structure is highly conserved and includes a short N-terminal amino acids stretch, an alpha helical transmembrane domain and a carboxy terminal region (Torres et al., 2007).

E protein is incorporated at a low copy number in the viral envelope (Maeda et al., 2001; Raamsman et al., 2000). Nevertheless, high amounts of E protein are accumulated within cells during viral infection, suggesting an important role of this protein during virus cycle. CoV E protein mainly distributes between ER and Golgi apparatus membranes where it actively participates in virus budding, morphogenesis and trafficking (Corse and Machamer, 2000; Lim and Liu, 2001; Nal et al., 2005; Nguyen and Hogue, 1997; Raamsman et al., 2000; Ruch and Machamer, 2012a). Particularly, SARS-CoV E protein mainly localizes in the endoplasmic reticulum–Golgi intermediate compartment (ERGIC) when expressed alone or during virus infection (Nieto-Torres

* Corresponding authors.
E-mail addresses: aguilell@uji.es (V.M. Aguilella), L.Enjuanes@cnb.csic.es (L. Enjuanes).
[1] Both authors equally contributed to this work.

0042-6822/$ - see front matter © 2012 Elsevier Inc. All rights reserved.
http://dx.doi.org/10.1016/j.virol.2012.07.005

et al., 2011). It has been proposed that SARS-CoV E protein sequesters protein associated with lin seven 1 (PALS1), a member of the tight junctions complex, to the ERGIC, disrupting the epithelia and possibly contributing to the lung damage observed in SARS patients (Teoh et al., 2010). The presence of SARS-CoV E protein at the cell plasma membrane has been previously suggested (Pervushin et al., 2009), however, these results have not been confirmed in recent studies (Nieto-Torres et al., 2011).

CoV E protein self-associates forming an oligomeric structure that delimits an ion conductive pore in planar lipid bilayers and micelles (Pervushin et al., 2009; Torres et al., 2006; Wilson et al., 2006, 2004). Synthetic CoV E proteins of human coronavirus 229E (HCoV-229E), mouse hepatitis virus (MHV), SARS-CoV and avian infectious bronchitis virus (IBV), behaved as cation-selective channels when they were reconstituted into planar lipid bilayers. Furthermore, it has been reported that HCoV-229E (genus α CoV) E protein was more selective to K^+ than to Na^+, whereas MHV and SARS-CoV (genus β CoVs) and IBV (genus γ CoV) E proteins were more selective to Na^+ than K^+ ions (Wilson et al., 2006, 2004). Studies using SARS-CoV E protein derived peptides showed that the transmembrane domain had ion conductive properties (Torres et al., 2007; Wilson et al., 2004), and some crucial residues involved in this activity have been identified (Torres et al., 2007).

Generation of MHV recombinant viruses, in which E protein was interchanged by CoV genus α, β and γ E proteins indicated that only E proteins corresponding to genus β and γ could partially replace the function of MHV E protein (Kuo et al., 2006). It was speculated that the selectivity of the channel could be important for the functional replacement. However, the possible biological relevance of ion selectivity in different CoV E proteins requires additional studies.

Other RNA viruses also encode small transmembrane proteins with ion channel properties. Influenza virus M2, hepatitis C virus p7, human immunodeficiency virus (HIV) vpu, and poliovirus 2B proteins are some examples of a growing list of these virally encoded ion channels called viroporins (de Jong et al., 2006; Ewart et al., 1996; Pinto et al., 1992; Wozniak et al., 2010). It has been described that these proteins are involved in diverse processes such as virus entry, trafficking and maturation, inflammation, and apoptosis (Campanella et al., 2004; Ichinohe et al., 2010; Wozniak et al., 2010).

Deletion of E gene in different CoVs may result in a complete abrogation of virus maturation and release, as shown for transmissible gastroenteritis virus (TGEV) (Ortego et al., 2007, 2002) or in a reduction of virus growth, as described for MHV (Kuo and Masters, 2003) and SARS-CoV (DeDiego et al., 2007). In addition, a SARS-CoV lacking E gene (SARS-CoV-ΔE) was attenuated in three animal models (DeDiego et al., 2007, 2008; Netland et al., 2010). Experimental data comparing SARS-CoV-ΔE and the parental virus revealed that E protein reduced cellular stress and virus-induced apoptosis (DeDiego et al., 2011).

Some reports have revealed the importance of CoV E protein transmembrane domain in virus production and maturation. When alanine residues were introduced in the MHV E protein transmembrane domain, disrupting the alpha helix structure and repositioning polar residues, virus growth was compromised, suggesting an important function for E protein transmembrane domain in virus biogenesis (Ye and Hogue, 2007). Replacement of IBV E transmembrane domain by a heterologous one that lacked ion conductance activity resulted in a virus that was poorly secreted to the extracellular media (Ruch and Machamer, 2011).

In the present work we have characterized the ion conductive properties of the transmembrane domain of the SARS-CoV E protein, with or without amino acid substitutions, and the full-length E protein, aiming to determine the functions affected by SARS-CoV E protein ion channel activity. Residues N15 and V25 were essential for SARS-CoV E protein ion channel activity. In all cases where the bilayer membrane was permeabilized, the channel showed symmetric ion transport properties either for positive or negative applied voltages, and its conductance was not regulated by voltage. Interestingly, when E protein was reconstituted in negatively charged lipid bilayers, the ion channel became slightly more selective to cations than to anions. The transmembrane domain of HCoV-229E E protein was also analyzed as a putative K^+ selective channel. A very weak selectivity for K^+ over Na^+ was observed for this peptide and its small preference for cations was also regulated by the charge of the lipid membranes, as was the case of SARS-CoV E protein. We propose that lipids are an integral component of the CoV E protein derived ion channels, a novel finding for these structures.

Results and discussion

E protein conductance on neutral planar lipid bilayers

Previous studies attributed the ion channel activity of SARS-CoV E protein to the transmembrane domain of the protein (Torres et al., 2007; Wilson et al., 2004). In order to identify residues involved in ion channel activity, the spatial distribution of SARS-CoV Urbani strain E protein transmembrane domain amino acids was predicted by helical wheel modeling using Protean (DNASTAR Software, Lasergene) and information from nuclear magnetic resonance (NMR) studies (Pervushin et al., 2009) (Fig. 1). In addition, conserved amino acids located within the E protein transmembrane domain of different CoV species were identified by sequence alignment (Fig. S1, supplementary data). Using information from these sources, conserved polar amino acids located at the beginning and the end of the transmembrane domain, and conserved amino acids central to the CoV E protein transmembrane domain, which in many cases were tentatively located towards the lumen of the pore formed by SARS-CoV E protein, were mutated (Table 1 and Fig. 1). A total of nine peptides derived from SARS-CoV E protein were synthesized, one of them (*wt*) representing the wild type protein transmembrane domain and its flanking polar amino acids, and eight mutant peptides including different residue substitutions. One (M2 to M7), two (M1) or four (M8) amino acids were replaced in each peptide at different positions along the transmembrane domain, or at both the amino- or carboxy-termini of this domain (Table 1 and Fig. 1).

The ion channel activity of these peptides was evaluated by electrophysiological measurements in artificial lipid bilayers. Single channel conductance was estimated from a statistical analysis of the current jump amplitudes, not from the total current measured. This procedure allows a reliable estimate of the most probable value of current change every time a new channel is inserted or disappears. Although several channels are being inserted, the magnitude of the current through a single channel could be discriminated. In order to exclude any peptide–lipid or peptide–peptide electrostatic interactions previous to peptide insertion (Sani et al., 2012), measurements were initially made in neutral lipid DPhPC bilayers. Six of the peptides investigated were able to permeabilize the phospholipid membrane. *Wt* as well as mutant peptides M1, M2, M5, M6 and M7 led to spontaneous current bursts 10–15 min after the peptide was added to the *cis* chamber (Fig. 2A). These results indicated that residues E7 and E8 (mutated in M1 peptide), T11 (mutated in M2 peptide), T30 (mutated in M5 peptide), T35 (mutated in M6 peptide) and R38 (mutated in M7 peptide) were not completely essential for the ion channel activity of SARS-CoV E protein derived peptides. M1, M5 and M7 peptides displayed conductance

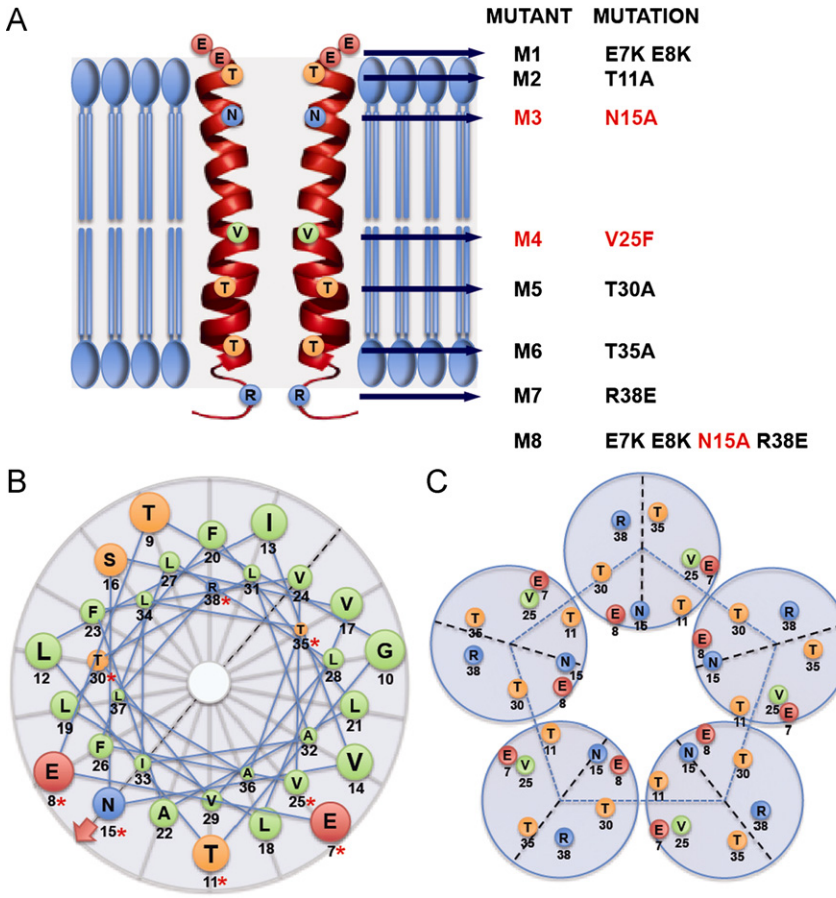

Fig. 1. Representation of SARS-CoV E protein transmembrane domain showing the location of the mutated residues. (A) Cartoon representing two of the several monomers of E protein transmembrane domain inserted in a lipid bilayer. Circles over the alpha helices indicate the predicted location of the mutated amino acids. Red circles denote negatively charged polar amino acids; blue circles denote positively charged polar amino acids; orange circles correspond to uncharged polar amino acids; and green circles represent nonpolar amino acids. Capital letters in the alpha helix are used for the amino acids that have been substituted. The mutant and mutations columns on the right side show the mutant name and their corresponding substitutions. Numbers and letters in red show mutants and mutations, previously described as critical for ion channel activity (Torres et al., 2007). (B) Alpha helix wheel modeling of SARS-CoV E protein transmembrane domain and flanking amino acids: Top view of an E peptide monomer, showing the spatial distribution of the different amino acids. Numbers represent the position of the amino acid in the SARS-CoV E protein sequence. Asterisks indicate the amino acids mutated in this work. Red arrow points to the lumen of the pore determined by E peptide oligomerization, as previously described for N15 in micelles (Torres et al., 2007). (C) Top view representation of a hypothetical pentameric E peptide ion channel. The position of the mutated amino acids within E monomers are shown in a plane perpendicular to the pore axis.

Table 1
Sequence of coronavirus E protein peptides representing the transmembrane domain and closely flanking amino acids.

Peptide	Sequence
	10 15 20 25 30 35[a]
wt	EETGTLIVNSVLLFLAFVVFLLVTLAILTALR
M1	[b]**KK**TGTLIVNSVLLFLAFVVFLLVTLAILTALR
M2	EETG**A**LIVNSVLLFLAFVVFLLVTLAILTALR
M3	EETGTLIV**A**SVLLFLAFVVFLLVTLAILTALR
M4	EETGTLIVNSVLLFLAFV**F**FLLVTLAILTALR
M5	EETGTLIVNSVLLFLAFVVFLLV**A**LAILTALR
M6	EETGTLIVNSVLLFLAFVVFLLVTLAIL**A**ALR
M7	EETGTLIVNSVLLFLAFVVFLLVTLAILTAL**E**
M8	**KK**TGTLIV**A**SVLLFLAFVVFLLVTLAILTAL**E**
HCoV-229E	DDHALVVNVLLWCVVLIVILLVCITIIKLIK

[a] Bar indicates the location of SARS-CoV and HCoV-229E E proteins predicted transmembrane domain.
[b] Residues in bold represent the mutated amino acids.

values similar to the *wt* peptide, suggesting that these mutations did not dramatically alter the pore conformation. Interestingly, mutations T11A (present in M2 peptide) and T35A (present in M6 peptide) led to currents of higher intensity than that induced by the *wt* peptide. In the absence of further structural information, we could speculate that these mutations may lead to a wider pore.

In contrast, three of the mutant peptides studied, M3, M4 and M8, did not permeabilize the bilayer (Fig. 2B). In the case of M3, M4 and M8 peptides, which did not show spontaneous channel activity, a negative potential of increasing magnitude (up to 130 mV) was applied to check whether their insertion into the lipid membrane could be facilitated. However, no change in channel activity was found for these peptides by increasing voltage differences between chambers (data not shown). In order to ensure that mutants M3, M4 and M8 peptides did not display any ion channel activity, 0.5–1 μl of a 300 μg/ml solution of these synthetic peptides were added to the *cis* chamber and registers were made during 10–15 min. After this time, 0.5–1 μl of a 300 μg/ml solution were added successively and the process was repeated at least 15 times in order to check the absence of ion channel activity. No ion conductance was observed (data not shown), strongly suggesting that substitutions N15A (mutated in M3 and M8 peptides) and V25F (mutated in M4 peptide) totally inhibited SARS-CoV E ion channel activity. These data are in agreement with previously reported results using a peptide corresponding to the transmembrane domain of SARS-CoV E

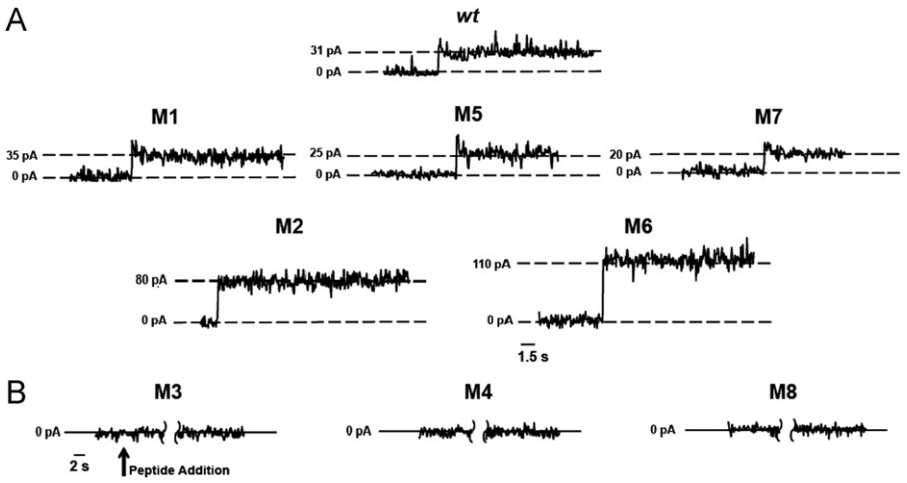

Fig. 2. Ionic current recordings of peptides derived from SARS CoV E protein transmembrane sequence with different mutations. Current was measured in 1 M KCl at pH 6. *wt*-E and mutant peptides M1, M2, M5, M6 and M7 showed the indicated ion channel activity under an applied voltage of 100 mV (A), whereas mutants M3, M4 and M8 did not permeabilized the membrane (B).

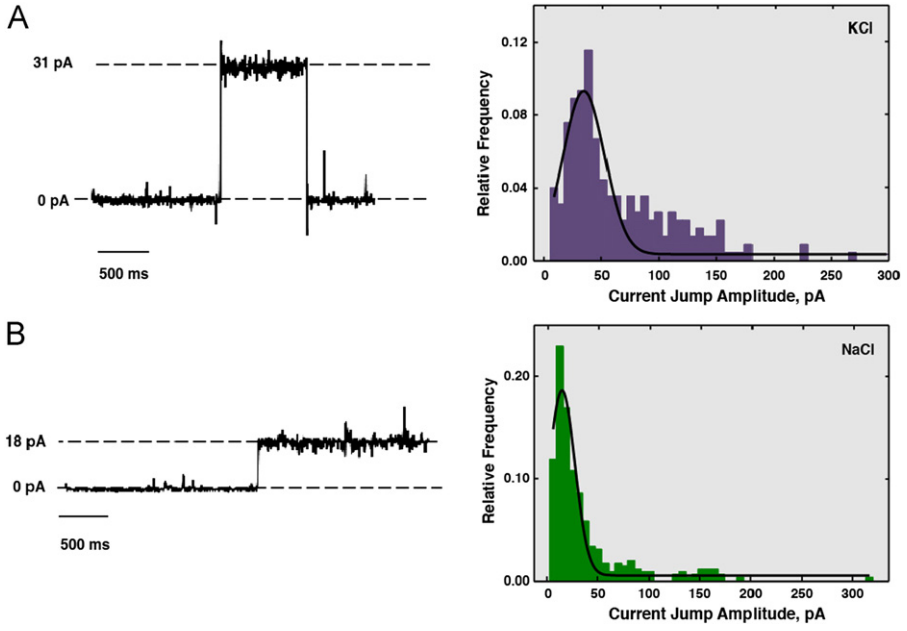

Fig. 3. Ionic current through the *wt*-E peptide channel in a DPhPC membrane. (A) Sample recording of a single channel event (left) and histogram of current jump amplitude in 1 M KCl (right). (B) Recording of a single channel insertion (left) and histogram of current jump amplitude in 1 M NaCl (right). Histograms comprise values from 300 recording events.

protein flanked by two lysine residues (Torres et al., 2007). Coronavirus E protein ion channel activity has been related with virus production and secretion (Ye and Hogue, 2007). Modifications by alanine scanning insertion mutagenesis of the E protein transmembrane domain of mouse hepatitis coronavirus, resulted in mutant viruses which exhibited smaller plaque phenotypes, and their production was significantly reduced (between 10- and 100-fold). It is interesting to note that mutation of the SARS-CoV E protein amino acid N15 performed in our study, knocking down the ion channel activity, is equivalent to amino acid T16 of infectious bronchitis coronavirus (IBV) (Ruch and Machamer, 2012b). This amino acid is essential for the disruption of the secretory pathway in IBV infected cells but has a limited effect on virus assembly as judged by virus-like particle production, suggesting that secretory pathway disruption and virus assembly are independent activities. In agreement with these results, introduction of amino acid substitutions N15A and V25F within the E protein of a recombinant SARS-CoV led to a slight reduction (lower than five-fold) of virus titers in cultured Vero E6 cells (data not shown). Extrapolation of these results, obtained with the two CoVs, could suggest that ion channel activity of E protein may be required to disrupt the secretory pathway during CoV infection but that it has low impact on virus titers in cells in culture. The introduced changes (single amino acid substitutions) had a lower effect on virus titers as compared with MHV E protein alanine insertion mutants reported in the work by Ye and Hogue (2007), which probably had a higher impact on the structure of E protein and, as consequence, a significant effect on virus production.

To further characterize the ion channel activity of *wt*-E peptide, current traces corresponding to 300 events were measured both in 1 M KCl and 1 M NaCl under an applied voltage of +100 mV (Fig. 3A and B, respectively). Histograms of the current jump amplitudes of the recorded traces showed that the most frequent

events corresponded to single channel conductances of 0.31 ± 0.12 nS and 0.18 ± 0.12 nS in KCl and NaCl, respectively (Fig. 3A and B, respectively, right panels) indicating that the peptide derived from SARS-CoV E protein transmembrane domain behaved as an ion channel either in KCl and NaCl solutions. These results almost matched the ones obtained using a full-length SARS-CoV E synthetic protein (0.37 ± 0.16 nS and 0.19 ± 0.06 nS for KCl and NaCl, respectively) (data not shown), further validating the use of the transmembrane domain derived peptides to measure the ion channel activity of SARS-CoV E protein. The conductance results obtained in KCl and NaCl solutions showed no enhanced selectivity of E protein for K^+ than for Na^+. Indeed, the higher conductance shown for KCl ($\sim$1.7 times larger than in NaCl) in Fig. 3A is due to the intrinsic properties of these electrolytes, as the mobility of K^+ is 1.66 times higher than the mobility of Na^+. Interestingly, a few current jump amplitudes were observed in 1 M KCl with values multiple of the most frequent current step of 31 pA (18% of these currents to double and 10% to triple) (Fig. 3A, right panel). In NaCl solutions, these events were rare, as jump amplitudes double or triple of the most frequent one were only 5% and 3%, respectively (Fig. 3B, right panel). These results suggested that high conductance states could be actually originated by occasional simultaneous insertion of two or three channels rather than by wider independent structures.

To analyze whether SARS-CoV E protein behaves as a voltage-gated ion channel, its ion channel activity was measured under different voltages. Single channel current–voltage (I–V) curves (Fig. 4) exhibited an ohmic behavior and therefore, a voltage independent conductance. The linear intensity to voltage (I–V) relationship revealed that the number of current carriers did not depend on the direction of the applied voltage difference and, therefore, the channel displayed symmetric ion transport properties when positive or negative voltage differences were applied. These results indicated that SARS-CoV E protein ion channel activity was not regulated by the applied electric potential. This constitutes a distinctive trend at odds with other channel forming peptides like alamethicin (Hall et al., 1984) or syringomycin E (Malev et al., 2002), which display voltage dependent current that has been linked to the existence of several conformational states. The fact that SARS-CoV *wt*-E peptide exhibited the same conductance regardless of the applied voltage discards the existence of voltage-induced dynamical structures and provides some support to the hypothesis that the variety of high conductance states found in Fig. 3A and B were actually originated by clusters of small structures and not by different conformational states.

Conductance of native E peptide ion channel in polar membranes

To examine the influence of a charged lipid on the *wt*-E channel properties, current recordings in a negatively charged DPhPS membrane were performed. The histograms of the *wt*-E peptide channel conductance in pure DPhPS membranes point to a single channel conductance of 0.15 ± 0.01 nS in 1 M KCl (Fig. 5). The comparison with Fig. 3A indicates that the host lipid not only determines the width of the conductance histograms but also the single channel conductance. Thus, the distribution of current jump amplitudes for the *wt*-E peptide in DPhPS charged membranes was much narrower than in neutral DPhPC membranes, suggesting that simultaneous multi-channel insertions were rare events when the peptide was reconstituted in DPhPS. But more important is the fact that the *wt*-E peptide channel conductance in a negatively charged lipid is less than half the value in a neutral membrane. This cannot be explained exclusively by the electrostatic interactions arising from the surface charge of the lipid membrane. The accumulation of ions near the pore entrance due to the membrane surface charge should give just the opposite effect, i.e., greater channel conductance in DPhPS, as occurs in alamethicin (Aguilella et al., 2011). Our results suggest that lipids are much more than inert scaffolds but they are functionally involved in the channel formation so that the observed dependence of *wt*-E channel conductance on the lipid type could be associated to the existence of different conformations in such a way that the aqueous pore in DPhPS membranes is narrower than in DPhPC membranes. Therefore, we can reasonably hypothesize that *wt*-E peptides induce permeabilization changes in membranes via the formation of protein–lipid pores, and lipid polar

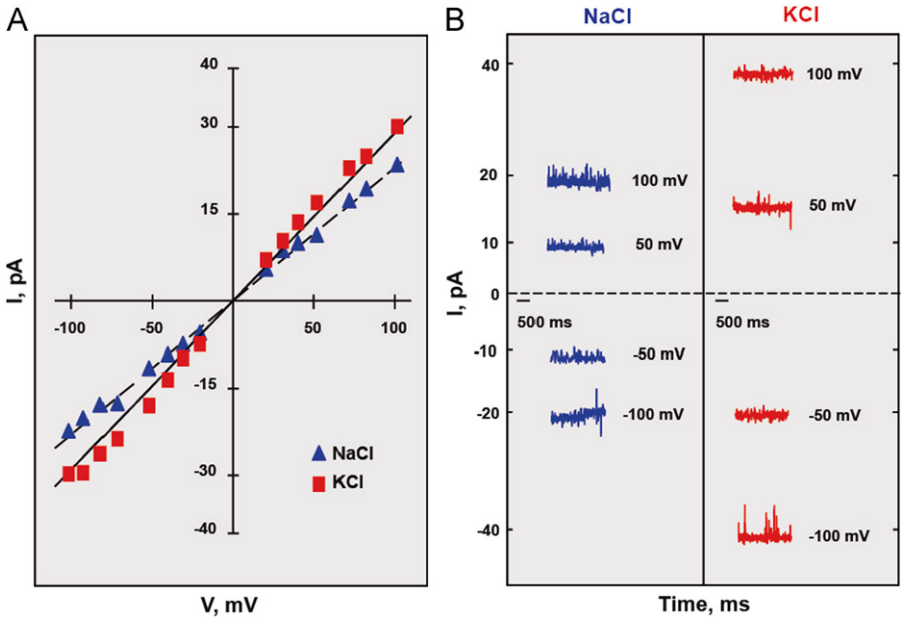

Fig. 4. *wt*-E peptide voltage independent current. (A) *wt*-E peptide showed a linear current–voltage relationship in 1 M NaCl (triangles) and 1 M KCl (squares) solutions. Each point of the I–V plot represents the mean of at least three current readings. Error bars were smaller than the symbol size. The line is a linear regression fit of data points. (B) Traces recorded several minutes after the membrane was held at the indicated potential under same conditions than panel A. Traces were filtered at 100 Hz by a digital eight-pole Bessel low pass filter (Clampfit 10.2, Molecular Devices). Smaller conductances correspond to NaCl.

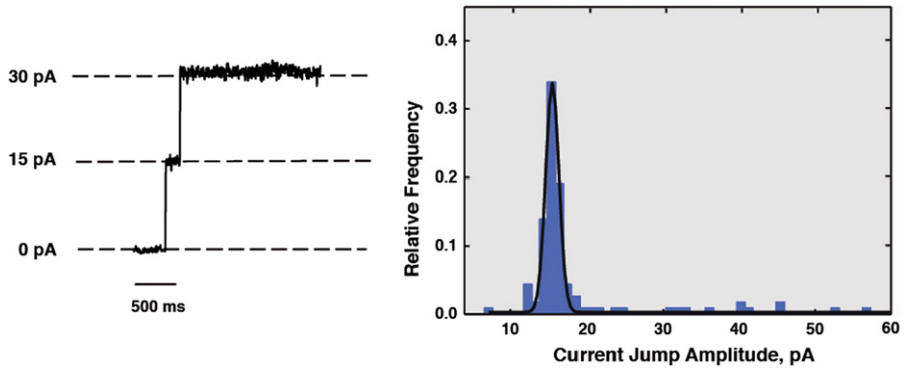

Fig. 5. Ionic current through the *wt*-E peptide channel in a DPhPS membrane. Sample recording of a single channel event and the subsequent insertion of another channel (left) and histogram of current jump amplitude in 1 M KCl (right). Histograms comprise values from 300 recording events.

Table 2
Reversal potential of native SARS-CoV transmembrane *wt*-E peptide in artificial membranes with different lipid bilayer composition under a 10-fold concentration gradient.

%DPhPS	NaCl[a]		KCl[c]	
	E_{rev} (mV)	P_+/P_-[b]	E_{rev} (mV)	P_+/P_-[b]
0	12.2 ± 2.0 ($n=59$)	0.6 ± 0.1	1.9 ± 0.8 ($n=20$)	1.0 ± 0.1
20	-7.7 ± 0.6 ($n=7$)	1.4 ± 0.1	-19.9 ± 0.8 ($n=7$)	2.7 ± 0.1
50	-11.8 ± 2.4 ($n=7$)	2.0 ± 0.2	-27.3 ± 2.4 ($n=7$)	3.9 ± 0.5
100	-26.6 ± 3.5 ($n=10$)	3.8 ± 0.7	-35.8 ± 2.0 ($n=10$)	6.6 ± 0.9

[a] NaCl and [c]KCl concentrations of 500 mM in *cis* chamber and 50 mM in *trans* chamber were used.
[b] P_+/P_-, ratio of the permeability to positive versus negative ions.

Table 3
Reversal potential measured for SARS-CoV full-length E protein in planar bilayer membranes with different lipid composition under a 10-fold concentration gradient.

%DPhPS	NaCl[a]		KCl[c]	
	E_{rev} (mV)	P_+/P_-[b]	E_{rev} (mV)	P_+/P_-[b]
0	8.6 ± 1.7 ($n=10$)	0.7 ± 0.1	-5.6 ± 1.4 ($n=15$)	1.1 ± 0.1
100	-34 ± 2 ($n=6$)	5.8 ± 0.4	-43 ± 3 ($n=10$)	10.5 ± 0.9

[a] NaCl and [c]KCl concentrations of 500 mM in *cis* chamber and 50 mM in *trans* chamber were used.
[b] P_+/P_-, ratio of the permeability to positive versus negative ions.

heads line totally or partially the pore wall together with several peptide monomers.

Modulation of E peptide ion selectivity by lipid bilayer composition

The reversal potential (E_{rev}) is defined as the applied transmembrane voltage that yields zero electric current when there is a concentration gradient across the membrane. E_{rev} is the method of choice to quantify selectivity for the sake of simplicity: the sign of the E_{rev} provides a quick estimation of the channel selectivity and its preference for cations or anions (Aguilella et al., 2011; Hille, 2001). The measured E_{rev} can be converted into the channel permeability (P_+/P_-) by means of the Goldman–Hodgkin–Katz (GHK) (Hodgkin and Katz, 1949) equation, being P_+ cation permeability and P_- anion permeability.

E_{rev} was measured under a 10-fold salt gradient (500 mM/50 mM KCl, and 500 mM/50 mM NaCl) with different lipid bilayer compositions. In planar membranes of neutral lipid DPhPC the native E peptide channel permeability ratios were $P_+/P_- = 0.6 \pm 0.1$ for NaCl and $P_+/P_- = 1 \pm 0.1$ for KCl (Table 2, first row). The interpretation of these permeability ratios must take into account that P_+/P_- is a joint measure of the channel discrimination between ions with different charge (electrostatic exclusion or accumulation) and the electrolyte intrinsic properties (difference between cation and anion mobility). This means that in a hypothetical neutral pore devoid of any interaction, the corresponding cation/anion permeability ratios, which represent the ratio of the diffusion coefficients in a free solution, should be $P_+/P_- \sim 0.5$ for NaCl and $P_+/P_- \sim 1$ for KCl. Thus, the calculated P_+/P_- ratios in the first row of Table 2 offer two interesting conclusions. On one hand, the *wt*-E peptide induced channels in DPhPC bilayers behaved almost like a neutral pore because they did not discriminate cations over anions. On the other hand, the observed differences between P_+/P_- ratios for NaCl or KCl in the first row of Table 2 reflects the different mobility of Na^+ and K^+, indicating that the channel has no specificity for Na^+ or K^+ (Alcaraz et al., 2009).

The observed lack of selectivity is in apparent contradiction with previous studies reporting that the N-terminal 40 amino acids of SARS-CoV E protein forms cation selective channels (Wilson et al., 2004). However, it is important to note that in those experiments, E transmembrane peptide was inserted in a lipid mixture with a 20% of a negatively charged lipid, instead of the neutral lipid bilayer used in the above reported experiments (Table 2, first row). Having in mind the crucial role that the lipid has on the channel conductance (compare Figs. 3A and 5), new series of reversal potential measurements were performed using a lipid mixture of DPhPC (neutral lipid): DPhPS (negatively charged lipid) (4:1) so as to mimic the lipid membrane charge density used by Wilson et al. (2004). In these charged membranes, permeability ratios were $P_+/P_- = 1.4 \pm 0.1$ for NaCl and $P_+/P_- = 2.7 \pm 0.1$ for KCl (Table 2, second row), showing that the ion channel was between two and three-fold more permeable to cations (Na^+ and K^+) than in the neutral lipid bilayer. Higher percentages of DPhPS within the lipid bilayer, further increased permeability ratios for NaCl and KCl, being $P_+/P_- = 2.0 \pm 0.2$ for NaCl and $P_+/P_- = 3.9 \pm 0.5$ for KCl in 50% DPhPS membranes, and $P_+/P_- = 3.8 \pm 0.7$ for NaCl and $P_+/P_- = 6.6 \pm 0.9$ for KCl in 100% DPhPS membranes (Table 2), indicating that the channel permeability was between three- and four-fold higher to Na^+ and K^+ than to Cl^- ions in 50% DPhPS membranes and between six and seven times more permeable to Na^+ and K^+ than to Cl^- ions in 100% DPhPS membranes (Table 2, last row). Overall, these data showed that the charge of the lipid modulated the ionic selectivity of the peptide channel. Equivalent results were obtained with the full-length SARS-CoV E protein (Table 3). When the lipid bilayer was constituted by DPhPC uncharged lipids permeability ratios were $P_+/P_- = 0.7 \pm 0.1$ for NaCl and $P_+/P_- = 1.1 \pm 0.1$ for

KCl, whereas when E protein was inserted in DPhPS negatively charged lipids permeability ratios increased to $P_+/P_- = 5.8 \pm 0.4$ for NaCl and $P_+/P_- = 10.5 \pm 0.9$ for KCl. These data indicated that lipid charge influenced E protein ion channel selectivity, as shown above for E protein derived peptide.

This mild selectivity is consistent with the fact that in all cases the peptides form relatively wide pores in which the interaction of the permeating ions with the channel residues is weak and the electrodiffusion of ions across the channel is not very different from bulk solution.

In previous studies (Wilson et al., 2006) it has been suggested that HCoV-229E envelope protein was assembled in ion channels with a preference for K^+ over Na^+. To further study if the influence of the artificial membrane polarity on the ion channel activity is a general issue for other CoV E proteins, we measured the selectivity of channels formed by a synthetic peptide having the same amino acid sequence than the transmembrane domain of HCoV-229E E protein in neutral lipid membranes (Table 4). Permeability ratios (P_+/P_-) were 1.1 ± 0.1 for NaCl and 2.5 ± 0.3 for KCl, indicating that the channel formed by HCoV-229E E protein was more permeable to cations than to anions in DPhPC. In addition to its mild cationic selectivity, the channel showed a slight preference for K^+ over Na^+ ions. In experiments with membranes formed by negatively charged DPhPS, the channel cationic selectivity increased up to a P_+/P_- ratio of 3.1 ± 0.2 for NaCl and 6.2 ± 0.9 for KCl, also showing a slight preference for K^+ over Na^+ (Table 4). Therefore, there is an increase in the channel cationic selectivity in DPhPS with respect to DPhPC. This indicates that the lipid charged head groups modulated the ion specificity, similarly to what has been shown above for SARS-CoV E peptide and full-length protein.

Apparently, reversal potential measurements (Tables 2–4) could lead to the conclusion that the K^+ ions are preferred over Na^+ in all three channels (*wt*-E peptide, the full-length SARS-CoV E protein and HCoV-229E envelope protein), since permeability ratios are greater for KCl than for NaCl. We want to stress again (as done above in the discussion of Fig. 3A and B) that these small differences between E_{rev} measured in KCl and NaCl are only due to the electrolyte intrinsic properties (ion mobility). Actually, the difference between the E_{rev} values of columns 2 and 4 (Tables 2 and 3) is very close to 11.3 mV, which corresponds to the difference between NaCl and KCl diffusion potentials for a 10-fold concentration ratio in free solution (Alcaraz et al., 2009). Even in HCoV-229E E peptide where the difference between E_{rev} for KCl and NaCl seems a bit larger, the preference for K^+ over Na^+ is not significant at all (a factor 2.3–2.7, depending on the lipid charge) as shown in Table 4. Furthermore, it is worth to mention that the permeability ratios obtained here are very far from the values usually associated to specific selectivity. In the channel literature (Aguilella et al., 2011), to consider that a channel is specific to a certain ion, the permeability to other ions should be extremely low. For instance, potassium channels have a permeability ratio for K^+ over $Na^+ > 100{:}1$ and calcium channels select for Ca^{2+} over Na^+ with a ratio $> 1000{:}1$.

In conclusion, full-length SARS-CoV E protein and E protein transmembrane peptide, form non-voltage-gated ion channels. Mutations N15A and V25F disrupt this ion conductive property of the E protein transmembrane peptide. Interestingly, SARS-CoV E and HCoV-229E E protein derived peptide, when reconstituted in lipid membranes, behaved as ion channels with an activity highly influenced by the charge of the lipids. Marked differences in conductance and E_{rev} were observed for E protein ion channels depending on whether they were formed in neutral or charged lipid bilayers. Due to lipid head charge repulsion, lipids may change their spacing within a membrane. Therefore, in principle, we could not completely exclude that the lipid charge could have affected the structure of the pore and, as a consequence, its conductance. The results previously described, showed that channel conductance in fully negatively charged lipids (DPhPS) was much smaller than in neutral lipids (DPhPC). These results are consistent with a more tight arrangement of helices in the pore induced by a higher lipid lateral pressure. However, such a conformation (narrower pore) does not seem sufficient to explain the increased channel selectivity in membranes containing charged lipids (from +2 mV in DPhPC to −36 mV in DPhPS for KCl in the case of SARS-CoV E protein derived peptide; from −6 mV in DPhPC to −43 mV in DPhPS for KCl in the case of full-length SARS-CoV E protein; and from −19 mV in DPhPC to −35 mV in DPhPS for KCl in the case of HCoV-229E E protein derived peptide). The combined evidence from conductance and selectivity measurements is the basis of our suggestion that the pore is made both of peptide helices and lipid head groups. Most likely, lipid molecules assembled with the peptide oligomers, to form the channel, similarly to what has been described for ascecropin, magainin and dermaseptin channels (Oren and Shai, 1998). The reported oligomeric structure of the E protein based on NMR data (Pervushin et al., 2009) suggests that E derived channel is essentially different from a classical barrel-stave model where peptides are tightly assembled in parallel, defining a regular open pore. Indeed, E peptides self associate with a certain slope, defining an irregular pore with a clear constriction in the middle. This type of structure seems compatible with the insertion of lipid head groups within the wider domains of the oligomer. This functional involvement of lipids in the channel structure can be accomplished in different ways as it happens with antimicrobial peptides (Eleftheriou et al., 2009). In one of them, the toroidal pore structure represents a membrane-spanning pore lined with polar peptide surfaces as well as phospholipid head groups.

Protein–lipid pores formation is favored in membranes with positive curvature (Sobko et al., 2004). Indeed, when using lipids inducing negative curvature of membranes like phosphatidylethanolamine (PE), the probability of channel formation is lowered because the membrane positive curvature needed for proteolipidic pores becomes energetically unfavorable. To reinforce the concept of CoV E protein derived channel as a protein-lipid entity, ion channel activity of SARS-CoV E transmembrane peptide was measured in membranes containing PE and different amounts of negatively charged lipid PS. Two types of membranes were reconstituted: (i) membrane 1 (PE:PC:PS, 3:1:1), and (ii) membrane 2 (PE:PC:PS, 3:3:1). Channel insertion was significantly diminished under these conditions and amounts of peptide 10- to 15-fold higher than those used in PC or PC:PS membranes were needed to detect channel activity (data not shown). These data confirmed that E protein most likely formed a protein–lipid pore. It is noteworthy that even under these conditions, P_+/P_- values were 3.3 ± 0.2 and 2.3 ± 0.2 for membrane 1 (20% negatively charged lipids) and membrane 2 (14% negatively charged lipids), respectively, which revealed that, as previously shown for PC:PS membranes, lipid charge influenced

Table 4
Reversal potential measured for HCoV-229E E protein derived peptide in planar bilayer membranes with different lipid composition under a 10-fold concentration gradient.

%DPhPS	NaCl[a]		KCl[c]	
	E_{rev} (mV)	P_+/P_-[b]	E_{rev} (mV)	P_+/P_-[b]
0	-2.4 ± 1.8 ($n=13$)	1.1 ± 0.1	-19 ± 4 ($n=24$)	2.5 ± 0.3
100	-17.4 ± 2.1 ($n=6$)	3.1 ± 0.2	-35 ± 4 ($n=15$)	6.2 ± 0.9

[a] NaCl and [c]KCl concentrations of 500 mM in *cis* chamber and 50 mM in *trans* chamber were used.

[b] P_+/P_-, ratio of the permeability to positive versus negative ions.

ion channel selectivity. The structure of these pores may also be a consequence of the direct interaction between specific domains of E protein monomers. Further work to clarify lipid–peptide channel conformation is in progress.

Finally, it has been described that CoV E protein locates within ERGIC/Golgi membranes of infected cells (Corse and Machamer, 2000; Lim and Liu, 2001; Nal et al., 2005; Nieto-Torres et al., 2011; Raamsman et al., 2000). These membranes are composed by lipid mixtures containing around 17% negatively charged lipids (van Meer et al., 2008). To analyze whether the effect of lipid charge on E protein ion channel selectivity may also happen in its physiological context, E protein derived ion channels were reconstituted in lipid membranes broadly mimicking ERGIC/Golgi membrane composition and charge: 59% dioleoyl phosphatidylcholine (DOPC), 24% dioleoyl phosphatidylethanolamine (DOPE) and 17% dioleoyl phosphatidylserine (DOPS). Ion channel selectivity was measured using a 10-fold KCl concentration gradient. Under these conditions, P_+/P_- was 3.3 ± 0.2, of the same order that the values previously obtained with membranes having 20% of the negatively charged lipid DPhPC (2.7 ± 0.1) (Table 2, right column), indicating that lipid charge influenced E protein ion selectivity in a more physiological context, and excluding major effects of lipid composition on ion selectivity. In such scenario, CoV E proteins integrated in lipid bilayers of subcellular compartments should behave more as channels with preference for cations.

Materials and methods

Peptide synthesis

The peptides corresponding to full-length SARS-CoV E protein, SARS-CoV E protein transmembrane domain (from residue 7 to 38) either in wild type or mutant versions, and HCoV-229E E protein transmembrane domain (from residue 7 to 37) were synthesized using standard solid phase FMOC chemistry peptide synthesizer (Intavis ResPep Gladbach, Germany). The peptides were cleaved from the resin with trifluoroacetic acid (TFA) and purified by high-performance liquid chromatography (HPLC). To this end, lyophilized peptides were dissolved in isopropanol and acetonitrile (3:2, v/v) at a final peptide concentration of ~5 mg/ml, and injected into a Zorbax SB-C18 9.4 mm × 250 mm column (Agilent) equilibrated with H_2O. Peptide elution was performed using a Waters 600 HPLC system and three solvents: A (94.9% H_2O, 5% acetonitrile, 0.1% trifluoroacetic acid), B (94.9% acetonitrile, 5% H_2O, 0.1% trifluroacetic acid) and C (94.9% isopropanol, 5% acetonitrile, 0.1% trifluoroacetic acid). The elution process started with 80% solvent A, 8% of solvent B and 12% of solvent C following a linear gradient to reach after 30 min a mixture of 40% solvent B and 60% solvent C. Finally, a gradient ending with a composition of 20% solvent B and 80% solvent C after 40 min was performed. The resulting fractions were pooled and lyophilized. Peptide purity was confirmed by mass spectrometry.

Ion channel reconstitution and ionic current recording

Planar bilayers were formed by apposition of two monolayers prepared from a solution of 1% pure diphytanoyl phosphatidylcholine (DPhPC), pure diphytanoyl phosphatidylserine (DPhPS), or a mixture of both lipids (Avanti polar lipids, Inc., Alabaster, AL) in pentane. Lipids were added on 70–90-μm diameter orifices in the 15-μm-thick Teflon partition that separated two identical chambers (Bezrukov and Vodyanoy, 1993; Montal and Mueller, 1972). The orifices were pretreated with a 1% solution of hexadecane in pentane. Aqueous solutions of KCl and NaCl were buffered with 5 mM HEPES at pH 6. All measurements were performed at room temperature (23 ± 1 °C). Ion channel insertion was achieved by adding 0.5–1 μl of a 300 μg/ml solution of synthetic protein or peptides in the buffer containing acetonitrile:isopropanol (40:60) on one side of the chamber (hereafter referred to as *cis* side).

An electric potential was applied using Ag/AgCl electrodes in 2 M KCl, 1.5% agarose bridges assembled within standard 250 μl pipette tips. The potential was defined as positive when it was higher on the side of the peptide addition (*cis* side), whereas the trans side was set to ground. An Axopatch 200B amplifier (Molecular Devices, Sunnyvale, CA) in the voltage-clamp mode was used to measure the current and the applied potential. The chamber and the head stage were isolated from external noise sources with a double metal screen (Amuneal Manufacturing Corp., Philadelphia, PA). The single-channel conductance was obtained from current measurements under an applied potential of +100 mV in symmetrical salt solutions of 1 M KCl and NaCl buffered with 5 mM HEPES at pH 6. The conductance values were evaluated using the Gaussian fit tool of Sigma Plot 10.0 (Systat Software, Inc).

The reversal potential, E_{rev}, was obtained as follows. First, a lipid membrane was formed at a given salt concentration gradient. Second, one or several channels were inserted into the bilayer and a net ionic current appeared due to the concentration gradient. Third, the ionic current through the channel was manually set to zero by adjusting the applied potential. The potential needed to achieve zero current was then corrected by the liquid junction potentials of the electrode salt bridges (Alcaraz et al., 2009) to obtain the E_{rev}. The measured E_{rev} was converted into the channel permeability (P_+/P_-) by means of the Goldman–Hodgkin–Katz (GHK) (Hodgkin and Katz, 1949) equation:

$$E_{rev} = \frac{RT}{F} \ln\left(\frac{P_+[A^+]_{trans} + P_-[B^-]_{cis}}{P_+[A^+]_{cis} + P_-[B^-]_{trans}}\right)$$

Acknowledgements

This work was supported by grants from the Ministry of Science and Innovation of Spain (MICINN. FIS2010-19810) and (BIO2007-60978 and BIO2010-16705), Fundació Caixa Castelló-Bancaixa (P1-1A2009-13), Generalitat Valenciana (Prometeu/2012/069), the European Community's Seventh Framework Programme (FP7/2007–2013) under the project "EMPERIE" EC Grant Agreement number 223498, and U.S. National Institutes of Health (NIH) (2P01AI060699-06A1, W000306844). CVB received a fellowship from UJI. JLN received a fellowship from CSIC. We thank Fernando Roncal (CNB, Proteomics facility) for peptides purification, and Marga Gonzalez for her technical assistance.

Appendix A. Supplementary material

Supplementary data associated with this article can be found in the online version at http://dx.doi.org/10.1016/j.virol.2012.07.005.

References

Aguilella, V.M., Queralt-Martin, M., Aguilella-Arzo, M., Alcaraz, A., 2011. Insights on the permeability of wide protein channels: measurement and interpretation of ion selectivity. Integr. Biol. (Camb.) 3, 159–172.

Alcaraz, A., Nestorovich, E.M., Lopez, M.L., Garcia-Gimenez, E., Bezrukov, S.M., Aguilella, V.M., 2009. Diffusion, exclusion, and specific binding in a large channel: a study of OmpF selectivity inversion. Biophys. J. 96, 56–66.

Arbely, E., Khattari, Z., Brotons, G., Akkawi, M., Salditt, T., Arkin, I.T., 2004. A highly unusual palindromic transmembrane helical hairpin formed by SARS coronavirus E protein. J. Mol. Biol. 341, 769–779.

Bezrukov, S.M., Vodyanoy, I., 1993. Probing alamethicin channels with water-soluble polymers. Effect on conductance of channel states. Biophys. J. 64, 16–25.

Campanella, M., de Jong, A.S., Lanke, K.W., Melchers, W.J., Willems, P.H., Pinton, P., Rizzuto, R., van Kuppeveld, F.J., 2004. The coxsackievirus 2B protein suppresses apoptotic host cell responses by manipulating intracellular Ca^{2+} homeostasis. J. Biol. Chem. 279, 18440–18450.

Chu, D.K., Peiris, J.S., Chen, H., Guan, Y., Poon, L.L., 2008. Genomic characterizations of bat coronaviruses (1A, 1B and HKU8) and evidence for co-infections in Miniopterus bats. J. Gen. Virol. 89, 1282–1287.

Corse, E., Machamer, C.E., 2000. Infectious bronchitis virus E protein is targeted to the Golgi complex and directs release of virus-like particles. J. Virol. 74, 4319–4326.

de Groot, R.J., Baker, S.C., Baric, R., Enjuanes, L., Gorbalenya, A.E., Holmes, K.V., Perlman, S., Poon, L., Rottier, P.J.M., Talbot, P.J., Woo, P.C.Y., Ziebuhr, J., 2012. Coronaviridae. In: King, A.M.Q., Adams, M.J., Carstens, E.B., Lefkowitz, E.J. (Eds.), Virus Taxonomy: Ninth Report of the International Committee on Taxonomy of Viruses. Elsevier Academic Press, San Diego, pp. 774–796.

de Jong, A.S., Visch, H.J., de Mattia, F., van Dommelen, M.M., Swarts, H.G., Luyten, T., Callewaert, G., Melchers, W.J., Willems, P.H., van Kuppeveld, F.J., 2006. The coxsackievirus 2B protein increases efflux of ions from the endoplasmic reticulum and Golgi, thereby inhibiting protein trafficking through the Golgi. J. Biol. Chem. 281, 14144–14150.

DeDiego, M.L., Alvarez, E., Almazan, F., Rejas, M.T., Lamirande, E., Roberts, A., Shieh, W.J., Zaki, S.R., Subbarao, K., Enjuanes, L., 2007. A severe acute respiratory syndrome coronavirus that lacks the E gene is attenuated in vitro and in vivo. J. Virol. 81, 1701–1713.

DeDiego, M.L., Nieto-Torres, J.L., Jimenez-Guardeno, J.M., Regla-Nava, J.A., Alvarez, E., Oliveros, J.C., Zhao, J., Fett, C., Perlman, S., Enjuanes, L., 2011. Severe acute respiratory syndrome coronavirus envelope protein regulates cell stress response and apoptosis. PLoS Pathog. 7, e1002315.

DeDiego, M.L., Pewe, L., Alvarez, E., Rejas, M.T., Perlman, S., Enjuanes, L., 2008. Pathogenicity of severe acute respiratory coronavirus deletion mutants in hACE-2 transgenic mice. Virology 376, 379–389.

Drexler, J.F., Gloza-Rausch, F., Glende, J., Corman, V.M., Muth, D., Goettsche, M., Seebens, A., Niedrig, M., Pfefferle, S., Yordanov, S., Zhelyazkov, L., Hermanns, U., Vallo, P., Lukashev, A., Muller, M.A., Deng, H., Herrler, G., Drosten, C., 2010. Genomic characterization of severe acute respiratory syndrome-related coronavirus in European bats and classification of coronaviruses based on partial RNA-dependent RNA polymerase gene sequences. J. Virol. 84, 11336–11349.

Drosten, C., Gunther, S., Preiser, W., van der Werf, S., Brodt, H.R., Becker, S., Rabenau, H., Panning, M., Kolesnikova, L., Fouchier, R.A., Berger, A., Burguiere, A.M., Cinatl, J., Eickmann, M., Escriou, N., Grywna, K., Kramme, S., Manuguerra, J.C., Muller, S., Rickerts, V., Sturmer, M., Vieth, S., Klenk, H.D., Osterhaus, A.D., Schmitz, H., Doerr, H.W., 2003. Identification of a novel coronavirus in patients with severe acute respiratory syndrome. N. Engl. J. Med. 348, 1967–1976.

Eleftheriou, D., Melo, M., Marks, S.D., Tullus, K., Sills, J., Cleary, G., Dolezalova, P., Ozen, S., Pilkington, C., Woo, P., Klein, N., Dillon, M.J., Brogan, P.A., 2009. Biologic therapy in primary systemic vasculitis of the young. Rheumatology 48, 978–986.

Enjuanes, L., Gorbalenya, A.E., de Groot, R.J., Cowley, J.A., Ziebuhr, J., Snijder, E.J., 2008. The Nidovirales. In: Mahy, B.W.J., Van Regenmortel, M., Walker, P., Majumder-Russell, D. (Eds.), Encyclopedia of Virology, third ed. Elsevier Ltd., Oxford, pp. 419–430.

Ewart, G.D., Sutherland, T., Gage, P.W., Cox, G.B., 1996. The Vpu protein of human immunodeficiency virus type 1 forms cation-selective ion channels. J. Virol. 70, 7108–7115.

Hall, J.E., Vodyanoy, I., Balasubramanian, T.M., Marshall, G.R., 1984. Alamethicin. A rich model for channel behavior. Biophys. J. 45, 233–247.

Hille, B., 2001. Ion Channels of Excitable Membranes, third ed. Sinauer Associates, Sunderland, MA.

Hodgkin, A.L., Katz, B., 1949. The effect of sodium ions on the electrical activity of giant axon of the squid. J. Physiol. 108, 37–77.

Huang, C., Ito, N., Tseng, C.T., Makino, S., 2006. Severe acute respiratory syndrome coronavirus 7a accessory protein is a viral structural protein. J. Virol. 80, 7287–7294.

Huang, C., Peters, C.J., Makino, S., 2007. Severe acute respiratory syndrome coronavirus accessory protein 6 is a virion-associated protein and is released from 6 protein-expressing cells. J. Virol. 81, 5423–5426.

Ichinohe, T., Pang, I.K., Iwasaki, A., 2010. Influenza virus activates inflammasomes via its intracellular M2 ion channel. Nat. Immunol. 11, 404–410.

Kuo, L., Hurst, K.R., Masters, P.S., 2006. Exceptional flexibility in the sequence requirements for coronavirus small envelope protein (E) function. J. Virol. 81, 2249–2262.

Kuo, L., Masters, P.S., 2003. The small envelope protein E is not essential for murine coronavirus replication. J. Virol. 77, 4597–4608.

Lim, K.P., Liu, D.X., 2001. The missing link in coronavirus assembly. Retention of the avian coronavirus infectious bronchitis virus envelope protein in the pre-Golgi compartments and physical interaction between the envelope and membrane proteins. J. Biol. Chem. 276, 17515–17523.

Maeda, J., Repass, J.F., Maeda, A., Makino, S., 2001. Membrane topology of coronavirus E protein. Virology 281, 163–169.

Malev, V.V., Schagina, L.V., Gurnev, P.A., Takemoto, J.Y., Nestorovich, E.M., Bezrukov, S.M., 2002. Syringomycin E channel: a lipidic pore stabilized by lipopeptide? Biophys. J. 82, 1985–1994.

Montal, M., Mueller, P., 1972. Formation of bimolecular membranes from lipid monolayers and a study of their electrical properties. Proc. Nat. Acad. Sci. U.S.A. 69, 3561–3566.

Muller, M.A., Paweska, J.T., Leman, P.A., Drosten, C., Grywna, K., Kemp, A., Braack, L., Sonnenberg, K., Niedrig, M., Swanepoel, R., 2007. Coronavirus antibodies in African bat species. Emerg. Infect. Dis. 13, 1367–1370.

Nal, B., Chan, C., Kien, F., Siu, L., Tse, J., Chu, K., Kam, J., Staropoli, I., Crescenzo-Chaigne, B., Escriou, N., van der Werf, S., Yuen, K.Y., Altmeyer, R., 2005. Differential maturation and subcellular localization of severe acute respiratory syndrome coronavirus surface proteins S, M and E. J. Gen. Virol. 86, 1423–1434.

Netland, J., DeDiego, M.L., Zhao, J., Fett, C., Alvarez, E., Nieto-Torres, J.L., Enjuanes, L., Perlman, S., 2010. Immunization with an attenuated severe acute respiratory syndrome coronavirus deleted in E protein protects against lethal respiratory disease. Virology 399, 120–128.

Nguyen, V.P., Hogue, B.G., 1997. Protein interactions during coronavirus assembly. J. Virol. 71, 9278–9284.

Nieto-Torres, J.L., Dediego, M.L., Alvarez, E., Jimenez-Guardeno, J.M., Regla-Nava, J.A., Llorente, M., Kremer, L., Shuo, S., Enjuanes, L., 2011. Subcellular location and topology of severe acute respiratory syndrome coronavirus envelope protein. Virology 415, 69–82.

Oren, Z., Shai, Y., 1998. Mode of action of linear amphipathic alpha-helical antimicrobial peptides. Biopolymers 47, 451–463.

Ortego, J., Ceriani, J.E., Patino, C., Plana, J., Enjuanes, L., 2007. Absence of E protein arrests transmissible gastroenteritis coronavirus maturation in the secretory pathway. Virology 368, 296–308.

Ortego, J., Escors, D., Laude, H., Enjuanes, L., 2002. Generation of a replication-competent, propagation-deficient virus vector based on the transmissible gastroenteritis coronavirus genome. J. Virol. 76, 11518–11529.

Perlman, S., Netland, J., 2009. Coronaviruses post-SARS: update on replication and pathogenesis. Nat. Rev. Microbiol. 7, 439–450.

Pervushin, K., Tan, E., Parthasarathy, K., Lin, X., Jiang, F.L., Yu, D., Vararattanavech, A., Soong, T.W., Liu, D.X., Torres, J., 2009. Structure and inhibition of the SARS coronavirus envelope protein ion channel. PLoS Pathog. 5, e1000511.

Pinto, L.H., Holsinger, L.J., Lamb, R.A., 1992. Influenza virus M2 protein has ion channel activity. Cell 69, 517–528.

Quan, P.L., Firth, C., Street, C., Henriquez, J.A., Petrosov, A., Tashmukhamedova, A., Hutchison, S.K., Egholm, M., Osinubi, M.O., Niezgoda, M., Ogunkoya, A.B., Briese, T., Rupprecht, C.E., Lipkin, W.I., 2010. Identification of a severe acute respiratory syndrome coronavirus-like virus in a leaf-nosed bat in Nigeria. MBio 1, e00208–00210.

Raamsman, M.J.B., Locker, J.K., de Hooge, A., de Vries, A.A.F., Griffiths, G., Vennema, H., Rottier, P.J.M., 2000. Characterization of the coronavirus mouse hepatitis virus strain A59 small membrane protein E. J. Virol. 74, 2333–2342.

Rota, P.A., Oberste, M.S., Monroe, S.S., Nix, W.A., Campganoli, R., Icenogle, J.P., Peñaranda, S., Bankamp, B., Maher, K., Chen, M.-H., Tong, S., Tamin, A., Lowe, L., Frace, M., DeRisi, J.L., Chen, Q., Wang, D., Erdman, D.d., Peret, T.C.T., Burns, C., Ksiazek, T.G., Rollin, P.E., Sanchez, A., Liffick, S., Holloway, B., Limor, J., McCaustland, K., Olsen-Rassmussen, M., Fouchier, R., Gunther, S., Osterhaus, A.D.M.E., Drosten, C., Pallansch, M.A., Anderson, L.J., Bellini, W.J., 2003. Characterization of a novel coronavirus associated with severe acute respiratory syndrome. Science 300, 1394–1399.

Ruch, T.R., Machamer, C.E., 2011. The hydrophobic domain of infectious bronchitis virus E protein alters the host secretory pathway and is important for release of infectious virus. J. Virol. 85, 675–685.

Ruch, T.R., Machamer, C.E., 2012a. The Coronavirus E protein: assembly and beyond. Viruses 4, 363–382.

Ruch, T.R., Machamer, C.E., 2012b. A single polar residue and distinct membrane topologies impact the function of the infectious bronchitis coronavirus E protein. PLoS Pathog. 8, e1002674.

Sani, M.A., Whitwell, T.C., Separovic, F., 2012. Lipid composition regulates the conformation and insertion of the antimicrobial peptide maculatin 1.1. Biochim. Biophys. Acta 1818, 205–211.

Schaecher, S.R., Mackenzie, J.M., Pekosz, A., 2007. The ORF7b protein of SARS-CoV is expressed in virus-infected cells and incorporated into SARS-CoV particles. J. Virol. 81, 718–731.

Shen, S., Lin, P.S., Chao, Y.C., Zhang, A., Yang, X., Lim, S.G., Hong, W., Tan, Y.J., 2005. The severe acute respiratory syndrome coronavirus 3a is a novel structural protein. Biochem. Biophys. Res. Commun. 330, 286–292.

Sobko, A.A., Kotova, E.A., Antonenko, Y.N., Zakharov, S.D., Cramer, W.A., 2004. Effect of lipids with different spontaneous curvature on the channel activity of colicin E1: evidence in favor of a toroidal pore. FEBS Lett. 576, 205–210.

Teoh, K.T., Siu, Y.L., Chan, W.L., Schluter, M.A., Liu, C.J., Peiris, J.S., Bruzzone, R., Margolis, B., Nal, B., 2010. The SARS coronavirus E protein interacts with PALS1 and alters tight junction formation and epithelial morphogenesis. Mol. Biol. Cell 21, 3838–3852.

Torres, J., Maheswari, U., Parthasarathy, K., Ng, L., Liu, D.X., Gong, X., 2007. Conductance and amantadine binding of a pore formed by a lysine-flanked transmembrane domain of SARS coronavirus envelope protein. Protein Sci. 16, 2065–2071.

Torres, J., Parthasarathy, K., Lin, X., Saravanan, R., Liu, D.X., 2006. Model of a putative pore: the pentameric alpha-helical bundle of SARS coronavirus E protein in lipid bilayers. Biophys. J. 91, 938–947.

van Meer, G., Voelker, D.R., Feigenson, G.W., 2008. Membrane lipids: where they are and how they behave. Nat. Rev. Mol. Cell Biol. 9, 112–124.
Wilson, L., Gage, P., Ewart, G., 2006. Hexamethylene amiloride blocks E protein ion channels and inhibits coronavirus replication. Virology 353, 294–306.
Wilson, L., McKinlay, C., Gage, P., 2004. SARS coronavirus E protein forms cation-selective ion channels. Virology 330, 322–331.
Wozniak, A.L., Griffin, S., Rowlands, D., Harris, M., Yi, M., Lemon, S.M., Weinman, S.A., 2010. Intracellular proton conductance of the hepatitis C virus p7 protein and its contribution to infectious virus production. PLoS Pathog. 6, e1001087.
Ye, Y., Hogue, B.G., 2007. Role of the coronavirus E viroporin protein transmembrane domain in virus assembly. J. Virol. 81, 3597–3607.